

Orbital fluctuation mechanism for superconductivity in iron-based compounds

Tudor D. Stanescu, Victor Galitski and S. Das Sarm a
 Condensed Matter Theory Center and Joint Quantum Institute,
 Department of Physics, University of Maryland, College Park, MD 20742-4111

We propose orbital fluctuations in a multiband ground state as the superconducting pairing mechanism in the new iron-based materials. We develop a general $SU(4)$ theoretical framework for studying a two-orbital model and discuss a number of scenarios that may be operational within this orbital fluctuation paradigm. The orbital and spin symmetry of the superconducting order parameter is argued to be highly non-universal and dependent on the details of the underlying band structure. We introduce a minimal two-orbital model for the Fe-pnictides characterized by non-degenerate orbitals that strongly mix with each other. They correspond to the iron d_{xy} orbital and to an effective combination of d_{zx} and d_{zy} , respectively. Using this effective model we perform RPA calculations of susceptibilities and effective pairing interactions. We find that spin and orbital fluctuations are, generally, strongly coupled and we identify the parameters that control this coupling as well as the relative strength of various channels.

PACS numbers:

I. INTRODUCTION

The recently discovered^{1,2,3,4,5,6,7,8} iron-based superconducting oxides with a transition temperature as high as 55K bring up the immediate important question of the mechanism underlying superconductivity in this new class of materials. An obvious temptation is to connect the superconductivity in these new materials to that in the high- T_c cuprates based on a number of compelling similarities: layered 2D nature of both classes of compounds, multi-element oxide nature of the materials in both cases, key role of doping with the undoped materials being non-superconducting, importance of nearby magnetic states whose suppression leads to superconductivity, relatively high superconducting transition temperatures. We argue here theoretically, using very general considerations, that in spite of these tantalizing similarities between the cuprates and the new Fe-based superconductors, there is a very important qualitative difference which suggests that the nature of superconductivity in the Fe-based oxides is likely to be different from that of the cuprates. In particular, the hallmark of the Fe-based superconductors seems to be the multiband nature of their low energy band structure as revealed by first principles band structure calculations^{9,10,11,12,13,14}, and as such, orbital fluctuations are likely to be a crucial ingredient of physics in these new materials. We propose in this article that the superconductivity in the Fe-based oxides is driven by novel orbital fluctuations (which are invariably coupled to the spin fluctuations, as described below) in the multiband ground state which have no analog in the standard model of the high- T_c cuprates. The existence of multiple bands at the Fermi surface gives rise to a new paradigm, namely, the possibility of a superconducting pairing mechanism driven by orbital fluctuations, which we believe are the underlying cause for the high-temperature superconductivity in these materials.

To explore the possibilities opened by this new paradigm we study an effective two-band tight-binding

model of the FeAs planes. Band structure calculations show that the electronic character near the Fermi level is mostly determined by the d-orbitals of Fe¹⁵ and that all *ve* orbitals participate in the formation of the Fermi surface¹². However, there are several reasons that make the study of a simple two-band effective model highly relevant: Firstly, a two-band model is the ideal minimal model that combines the requirements for observing multi-orbital physics with a relative simplicity that makes this physics transparent. Secondly, LDA-type calculations^{9,10,11,12,13,14} have shown that the undoped^{16,17,18,19} material is characterized by *ve* Fermi sheets: two quasi-2D electron pockets located near the M point of the Brillouin zone and two quasi-2D and one 3D hole pockets in the vicinity of the Γ point. However, upon electron doping the 3D hole pocket disappears and the 2D hole pockets shrink rapidly. Moreover, strong-coupling LDA+DMFT calculations¹⁵ show that at finite doping the bands responsible for the electron pockets clearly cross the Fermi level, while the hole pockets around the Γ point are barely identifiable. These preliminary results suggest that the low-energy physics responsible for superconductivity in the iron-based compounds may be governed by the two-bands associated with the electron pockets and, therefore, an effective two-band model would be an appropriate way to describe it. Nonetheless, as we show below, the nature of the orbitals that participate in the formation of these bands, as well as the strength and symmetry of the hybridization between them have direct consequences for the pairing mechanism. Furthermore, to completely clarify the key question of the relative importance of the electron and hole pockets in the low-energy physics of the FeAs layers as a function of doping, further calculations involving momentum-dependent self-energy effects are necessary.

The general analysis described in the next section has three main objectives. First, in order to disentangle and describe unambiguously various possible types of fluctuations we introduce a set of generators of the $SU(4)$ group

interaction operator $D = \sum_m C_{im}^y C_{im}^\#$ are generated in the charge channel, $X_i^{00} X_i^{00}$, the charge-orbital channel $X_i^{03} X_i^{03}$, as well as in the spin channel $X_i^{00} X_i^{00}$, and the spin-orbital channel $X_i^{33} X_i^{33}$. Consequently, there are distinct linear combinations of products of X -operators equal to D . Our choice is based on the following two conditions: i) the linear combinations of products of X -operators should be invariant under spin rotations, and ii) to each channel that generate a certain term of the interacting Hamiltonian we will ascribe a proportional fraction of the corresponding coupling constant. Using this procedure we obtain

$$\begin{aligned} {}^0(c) &= \text{diag} f(U + 2U^0 \quad J); \quad (U^0 + 2J + J^0); \\ &\quad (U^0 + 2J \quad J^0); \quad (U \quad 2U^0 + J)g \\ {}^0(s) &= \text{diag} f(U \quad J); \quad (U^0 \quad J^0); \\ &\quad (U^0 + J^0); \quad (U + J)g \end{aligned} \quad (6)$$

We begin our second task by classifying the pair operators $\hat{a}_{ab}(k)$ defined as linear combinations of products $C_{km}^y C_{km}^{y0}$. We choose combinations that are symmetric or antisymmetric under permutations of the spin (orbital) indices, representing the spin (orbital) triplet and singlet channels, respectively. In the notation $\hat{a}_{ab}(k)$ the first index refers to the orbital degree of freedom and takes the value $a = s$ for the orbital singlet and $a = 2, f_1, t_2, t_0, g$ for the orbital triplets. The spin index is $b = s$ for the spin singlet and $b = 2, f_1, t_2, t_0, g$ for the spin triplets. With these notation the 16 independent pair operators are

$$\begin{aligned} \hat{a}_{tm \quad t}(k) &= C_{km}^y C_{km}^y; \\ \hat{a}_{t_0=s \quad t}(k) &= \frac{1}{2} C_{k1}^y C_{k2}^y - C_{k2}^y C_{k1}^y; \\ \hat{a}_{t_m \quad t_0=s}(k) &= \frac{1}{2} C_{km}^y C_{km}^\# - C_{km}^\# C_{km}^y; \quad (7) \\ \hat{a}_{ab}(k) &= \frac{1}{2} s_1 C_{k1}^y C_{k2}^\# + s_2 C_{k1}^\# C_{k2}^y \\ &\quad + s_3 C_{k2}^\# C_{k1}^\# + s_4 C_{k2}^y C_{k1}^y; \end{aligned}$$

where $m = 2, f_1, 2g, 2, f^\#, \#g$ and the set of signs $(s_1; s_2; s_3; s_4)$ takes the values $(+; +; +; +)$ for $(ab) = (t_0 t_0)$, $(+; -; +; -)$ for $(ab) = (ts)$, $(+; +; -; -)$ for $(ab) = (st_0)$, and $(+; -; -; +)$ for $(ab) = (ss)$. Note that all the singlet-singlet and triplet-triplet pair operators are odd functions of momentum, $\hat{a}_{ss}(k) = -\hat{a}_{ss}(k)$ and $\hat{a}_{tt}(k) = -\hat{a}_{tt}(k)$, consequently pairing involving these operators occurs in the p-wave channel. On the other hand, the singlet-triplet and triplet-singlet pair operators are even functions of k , $\hat{a}_{st}(k) = \hat{a}_{st}(k)$ and $\hat{a}_{ts}(k) = \hat{a}_{ts}(k)$, and are involved in s-wave or d-wave pairing.

Using Eq. (7) we express the effective Hamiltonian (4) as

$$H_U^{\text{eff}} = \sum_{k, k^0} \sum_{a, b; a^0, b^0} \hat{a}_{ab \quad a^0 b^0}(k; k^0) \hat{a}_{ab}(k) \hat{a}_{a^0 b^0}^\dagger(k^0); \quad (8)$$

where, as usual, we retain only contributions of the form $C_{k_1 m_1 s_1}^y C_{k_2 m_2 s_2}^y C_{k_1 m_1 s_1}^0 C_{k_2 m_2 s_2}^0$ with $k_2 = k_1$ and $k_2^0 = k_1^0$. Because of the symmetry properties of the pair operators, most of the elements of the \hat{W} matrix are in fact zero. The non-vanishing elements are $W_{ss} = \hat{W}_{ss \quad ss}$ describing the pairing interaction in the orbital-singlet spin-singlet channel, $W_{st} = \hat{W}_{ss \quad t_0 t_0}$, with $t_0 = 2, f_1, t_2, t_0, g$, representing the orbital-singlet spin-triplet pairing, plus two 3×3 matrices $W_{tt} = \hat{W}_{t_0 t_0 \quad t_0 t_0}$ and $W_{ts} = \hat{W}_{t_0 t_0 \quad s s}$ corresponding to the orbital-triplet spin-triplet and orbital-triplet spin-singlet channels, respectively. Note the the coupling matrices are degenerate with respect to the spin-triplet label t_0 .

Next we express the pairing interaction W_{ab} in terms of the effective coupling constants ${}^{(c=s)}$. In order to simplify the expressions, we will take into consideration only the diagonal contributions ${}^{(c=s)}$ and ${}_{03}^{(c=s)} = {}_{30}^{(c=s)}$ which is always non-zero for non-degenerate orbitals, and assume that all the other coupling constants are negligible. With these assumptions, we have for the singlet-singlet and singlet-triplet channels

$$\begin{aligned} W_{ss} &= \frac{1}{16} \begin{pmatrix} 00 & 11 & 22 & 33 \end{pmatrix}; \\ W_{st} &= \frac{1}{16} \begin{pmatrix} + & + & + & + \\ 00 & 11 & 22 & 33 \end{pmatrix}; \end{aligned} \quad (9)$$

with ${}^+ = {}^{(c)} + {}^{(s)}$ and ${}^- = {}^{(c)} - {}^{(s)}$. The triplet-triplet pairing matrix becomes

$$W_{tt} = \begin{pmatrix} {}^{+}_{00} + {}^{+}_{11} & {}^{+}_{33} + {}^{+}_{22} & {}^{+}_{03} & 0 \\ {}^{+}_{11} & {}^{+}_{22} & {}^{+}_{00} + {}^{+}_{33} & 0 \\ 0 & 0 & {}^{+}_{00} + {}^{+}_{11} & {}^{+}_{22} + {}^{+}_{33} \end{pmatrix} \quad (10)$$

A similar expression can be written for the triplet-singlet channel, W_{ts} , by making the substitution ${}^+ \rightarrow {}^-$. Expressing the pairing interaction in terms of the effective coupling constants completes our second objective and provides the tools necessary for understanding orbital fluctuations mediated pairing.

Using the bare couplings 0 given by Eq. (6), the pairing interaction (9-10) becomes

$$\begin{aligned} W_{tt}^0 &= \begin{pmatrix} 0 & 0 & 0 \\ 0 & 0 & 0 \\ 0 & 0 & 0 \end{pmatrix}; \quad W_{ts}^0 = \frac{1}{2} \begin{pmatrix} U & J^0 & 0 \\ J^0 & U & 0 \\ 0 & 0 & U^0 + J \end{pmatrix}; \\ W_{ss}^0 &= 0; \quad W_{st}^0 = \frac{1}{2} (U^0 \quad J); \end{aligned} \quad (11)$$

At this level, pairing could only appear in the s-wave channel and have either orbital-triplet spin-singlet or orbital-singlet spin-triplet character. The necessary conditions are $U^0 < J$, or $U < J^0$. If we use parameters characterizing isolated Fe atoms, these conditions are certainly not satisfied, as $J; J^0 \gg U; U^0$. Even if we consider that the two-band effective model should contain renormalized values of these couplings, it is not very likely

that these conditions, especially $U < J^0$, be realized²¹. We conclude that, at the bare level, pairing is unlikely to occur. Theoretically, it may be realized only in the orbital-singlet spin-triplet channel if $U^0 < J^{22}$. The stability of this channel in the presence of fluctuations will be discussed in section IV.

Before discussing the role of fluctuations, we need to clarify the concepts of inter-orbital and inter-band pairing. In the absence of hybridization between orbitals, $t_{ij}^{mn} = 0$ (or $\gamma_{nm}(k) = 0$) for $n \notin m$, the wave-vectors k and k' characterizing pair operators of the type $c_{kn}^y c_{km}^y$ cannot be chosen to lie on the Fermi surfaces corresponding to the different orbitals, except when they are degenerate or at points of accidental degeneracies^{23,24}. The inter-pocket orbital-singlet spin-triplet pairing discussed in Ref. 23 corresponds to this situation. For the sake of clarity, we will use for this case the term inter-band pairing. In contrast, for a non-zero hybridization, the relevant momenta k and k' should be considered on the Fermi surface produced by the energy bands $E_n(k)$ obtained by diagonalizing H_t (not on the orbital "Fermi surfaces" generated by $\gamma_{nn}(k)$). Assuming inversion symmetry, the pair created by such an inter-orbital pair operator is well defined for any Fermi momentum. Note that diagonalizing the hopping Hamiltonian H_t is equivalent to performing a unitary transformation $\bar{U}(k)$. Using this transformation we can express orbital creation operators in terms of band creation operators as $c_{km}^y = \bar{U}_m(k) d_k^y$. Consequently, we can project the orbital pair operator into the low energy band and obtain a band pair operator relevant for the low-energy physics. Note that the two operators may have different symmetries²². To set the stage for our discussion of the orbital fluctuations, we conclude that, because the phase space available for inter-band pairing is in general very limited, this type of pairing is not likely to play a significant role in the mechanism responsible for superconductivity in the iron-based compounds. In contrast, inter-orbital pairing has no phase-space limitations and could be one of the key elements that characterizes the physics of these multi-orbital superconductors.

In the presence of hopping, the effective interactions $\chi^{(s)}$ will acquire a momentum dependence. For example, at the RPA level, the bare couplings (6) will be renormalized by the susceptibility $\chi(q) = \frac{1}{2} \sum_{m,n} \gamma_{mn}^0 \gamma_{mn}^0(k+q) G_{mn}^0(k) \gamma_{nn}^0(k)$, where $G_{nm}(k)$ is the Green function $\langle c_{kn}^y c_{km}^y \rangle$. It is convenient to express the elements of the susceptibility matrix in terms of $\gamma_{mn}^0 \gamma_{nn}^0(q) = \sum_k \gamma_{mn}^0(k+q) G_{nn}^0(k)$. The diagonal elements become

$$\begin{aligned} \chi_{00}(q) &= \frac{1}{2} (\epsilon_{11;11} + \epsilon_{12;21} + \epsilon_{21;12} + \epsilon_{22;22}); \\ \chi_{11}(q) &= \frac{1}{2} (\epsilon_{11;22} + \epsilon_{12;12} + \epsilon_{21;21} + \epsilon_{22;11}); \\ \chi_{22}(q) &= \frac{1}{2} (\epsilon_{11;22} - \epsilon_{2;12} - \epsilon_{1;21} + \epsilon_{22;11}); \end{aligned} \quad (12)$$

$$\chi_{33}(q) = \frac{1}{2} (\epsilon_{11;11} - \epsilon_{2;21} - \epsilon_{1;12} + \epsilon_{22;22});$$

The most significant off-diagonal components are $\chi_{03}(30) = (\epsilon_{11;11} - \epsilon_{2;21} - \epsilon_{1;12} - \epsilon_{22;22})/2$, which couple the spin susceptibility χ_{00} and the longitudinal orbital-spin component χ_{33} . Note that the rest of the off-diagonal components depend on contributions of the form $\epsilon_{ii;jj}$ or $\epsilon_{ij;jj}$ that are typically much smaller than the diagonal terms. Neglecting, for simplicity, the off-diagonal susceptibilities, the renormalized coupling constants become $\chi^{(s)}(q) = \chi^{(s)}(0) = 1 + \chi^{(s)}(q)$. Based on this expression, together with equations (6), (12) and (9-10) we identify three simple pairing scenarios. To establish the exact relation between these scenarios and the physics of the iron-based superconductors, detailed numerical calculations are necessary. Also, for certain values of the band and interaction parameters, more complicated situations that do not involve a certain dominant component of the susceptibility are possible (see Section IV).

Scenario A: $\epsilon_{nn;nn} \gg \epsilon_{nn;nm}; \epsilon_{nm;nm} \gg g$, i.e., the intra-orbital susceptibilities are dominant. This can be realized, for example, when the Fermi surface is characterized by an approximate nesting with wave-vector Q and the hybridization is negligible. The dominant elements of the susceptibility matrix are χ_{00} and χ_{33} . Considering the expression (6) of the bare interaction, we conclude that the strongest renormalization will occur in the spin channel, $\chi_{00}^{(s)}$, followed by the spin-orbital channel $\chi_{33}^{(s)}$ and the charge-orbital channel $\chi_{33}^{(c)}$. However, in the presence of any non-zero Hund's coupling J , the pure spin channel will dominate. This translates into a large negative contribution to $\chi_{00}^{(s)}(Q)$ or a large positive renormalization of $\chi_{00}(Q)$. Regardless of channel, spin fluctuations represent the driving force in this scenario. However, because χ_{03} is generally non-zero, spin fluctuations couple to the longitudinal spin-orbital fluctuations, thus enhancing $\chi_{33}^{(s)}$. Very importantly, this coupling between the spin and spin-orbital channels generates stronger fluctuations and, consequently, a stronger renormalization of the effective coupling constants in both channels. Notice that orbital fluctuations, which renormalize χ_{33} , give contributions to W_{st} and W_{ss} , as well as to W_{t_0t} and W_{t_0s} , which are opposite in sign to the contributions from the spin channel and, consequently, are detrimental to pairing. In contrast, for W_{tt} and W_{ts} , spin and orbital fluctuations have a similar effect on pairing. Considering also that in $\chi_{00}^{(s)}$ has a coefficient 3, while in $\chi_{33}^{(s)}$ the coefficient is +1, we conclude that the most likely pairing in this scenario is orbital-triplet spin-singlet pairing. This implies s-wave or d-wave symmetry for the order parameter.

Scenario B: $\epsilon_{nn;nn} \gg \epsilon_{nn;nm}; \epsilon_{nn;nm} \gg g$, i.e., the intra-orbital components are large and the hybridization is strong. In this case the off-diagonal terms $\epsilon_{nn;nm}$ contributing to χ_{00} and χ_{33} become important. The sign of these contributions at the relevant wave-vector Q de-

depends on the symmetry of the hybridization $\chi_{12}(\mathbf{k})$. A positive contribution will further enhance the spin fluctuations. On the contrary, a negative contribution makes χ_{33} larger than χ_{00} and this could offset the effect of the Hund's coupling J and promote the spin-orbital coupling $\chi_{33}^{(s)}$ as the main component of the pairing interaction. Pairing in this scenario is mainly mediated by either orbital fluctuations or spin fluctuations, depending on the sign of $e_{nm,pm}$, i.e., on the symmetry of the hybridization. Note that the key ingredient leading to the further enhancement of spin and spin-orbital fluctuations is the strong orbital hybridization. We emphasize that, in addition to the strength, a key role is played by the symmetry of the inter-orbital hybridization, as it determines the sign of the off-diagonal susceptibilities $e_{nm,pm}$. As in scenario A, the coupling constants that are most strongly renormalized are $\chi_{00}^{(s)}$ and $\chi_{33}^{(s)}$, leading to orbital-triplet spin-singlet pairing as the most likely type of pairing, with s- or d-wave symmetry for the order parameter.

Scenario C: $e_{nn,mm} = fe_{nn,pm}$; $e_{nm,pm} = g$, i.e., the inter-orbital components are larger than the intra-orbital contributions in the vicinity of certain relevant Q vectors. In this scenario the elements χ_{11} and χ_{22} of the susceptibility matrix become the dominant components. Consequently, the main contribution to the renormalized pairing interaction will come from the effective couplings χ_{11} and χ_{22} . The pairing mechanism is now controlled by orbital fluctuations, as in scenario B for negative off-diagonal susceptibilities $e_{nm,pm}$. However, this time it is the inter-orbital susceptibility that leads to a strong increase of the effective coupling in the charge-orbital and especially the spin-orbital channels. This will translate into a positive momentum-dependent contribution to the even-parity channels W_{st} and W_{t_0s} or a negative momentum-dependent contribution to the odd-parity channels W_{ss} and W_{t_0t} . However, because the $\chi_{33}^{(s)}$ contribution comes with a pre-factor -3, we can infer that always singlet-singlet or the triplet t_0 -singlet channels will be preferred over the triplet t_0 -triplet and the singlet-triplet channels, respectively.

III. EFFECTIVE TWO-ORBITAL MODEL

For a specific discussion of the orbital effects in Fe-pnictides, we need a simple tight-binding model that describes these materials. In particular, a choice of the hopping parameters in the non-interacting Hamiltonian (1) has to be made. In making this choice, we take into account the results of band structure calculations^{9,10,11,12,13,14} and try to reproduce as well as possible the low-energy sector. The goal is to reproduce not only the multi-pocket structure of the Fermi surface, but also the correct energy scales for the low-energy modes. We note here that effective two-orbital models have been already discussed in the literature^{25,26,27,28,29}, but they focus exclusively on the degenerate d_{zx} , d_{zy} or-

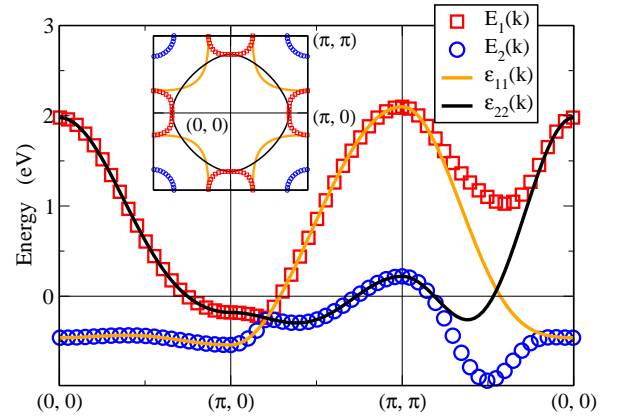


FIG. 1: (color online): Energy dispersion for the effective two-orbital model along the $(0;0) \rightarrow (\pi;0) \rightarrow (\pi;\pi) \rightarrow (0;0)$ path in momentum space. Orbital "1" corresponds to the iron d_{xy} orbital, while "2" corresponds to an effective $d_{zx} - d_{zy}$ combination. The dispersion of the second orbital is shown for a set of hopping parameters corresponding to the presence of a relatively large hole pocket (see main text). $E_{1(2)}(\mathbf{k})$ is the diagonalized high (low) energy band. Inset: Zero energy contours inside the unfolded Brillouin zone. The Γ point of the original Brillouin zone corresponds to $(0;0)$, $(\pi;\pi)$, while M corresponds to $(\pi;0)$, $(0;\pi)$.

bitals. However, d_{xy} is also known to play an important role in the formation of the electron pockets and it strongly mixes with the two degenerate orbitals. Potentially important aspects of pairing mechanism may occur because of this mixing between the d_{xy} orbital and either d_{zx} or d_{zy} , suggesting a three-orbital model for the Fe-pnictides²². Our goal is to capture some of this physics within a two-orbital model. Consequently, we consider an effective model of the Fe-based oxides consisting of two non-degenerate orbitals: the first corresponds to the iron d_{xy} orbital, while the second represents an "effective orbital" that simulates the combination of d_{zx} and d_{zy} . More precisely, the energy band associated with the second orbital approximates the low energy band structure of d_{zx} hybridized with d_{zy} .

The intra-orbital hopping parameters that define the model are $t_{ij}^{mm} = (t_{[0;0]}; t_{[\pi;0]}; t_{[\pi;\pi]}; t_{[0;\pi]})$, where $[x; y] = [(x_j - x_i); (y_j - y_i)]$ denotes a given hopping vector, as well as those related to it by symmetry. The first orbital is characterized by the set of hoppings $t_{ij}^{11} = (0.2; 0.32; 0.17; 0.015)$ eV. The proper energy scale is set by the nearest-neighbor hopping $t_{[\pi;0]} = 0.32$ eV^{13,30}. For the second orbital we use three different sets of parameters. If $t_{ij}^{22} = (0.18; 0.22; 0.16; 0.07)$ eV, a hole pocket is generated around the $\Gamma = (0;0)$ point (see Fig. 1). Again, the energy scale for the dispersion curve is determined by the choice of the nearest-neighbor hopping in accordance with the band structure calculations^{13,30}. For a smaller hole pocket, which would correspond to the doped case, we use $t_{ij}^{22} = (0.18; 0.22; 0.14; 0.05)$ eV. To simulate the case when the

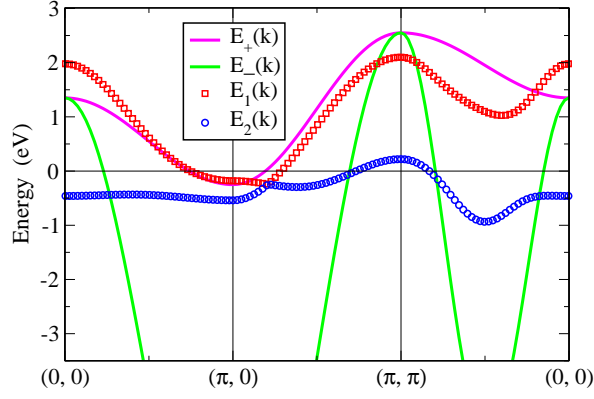


FIG. 2: (color online): Comparison of the band structure of our effective two-orbital model (E_1, E_2) with the band structure of the $d_{zx} - d_{zy}$ model from Refs. 25,26,27 (E_+, E_-) corresponding to a nearest-neighbor hopping $t_{ij} = 1$ eV and a chemical potential $\mu = 1.45$ eV. Notice the similarities between the high-energy bands E_1 and E_+ and the different energy scales of the lower energy bands.

hole pockets are absent, or have a very weak coherent spectral weight¹⁵, we use the set of hopping parameters $t_{ij}^{22} = t_{ij}^{22} = (0.18; 0.22; 0.125; 0.04)$ eV. Note that the only significant change in the dispersion curve occurs in the vicinity of the Γ point, where the hole pocket is located (for details, see the inset of Fig. 4). Finally, the hybridization between the two orbitals is described by $t_{12}(k) = 4 \sin k_x \sin k_y$ with $\mu = 0.25$ eV. The dispersion curves, diagonalized bands and zero energy contours are shown in Fig. 1. Note that our model reproduces the two electron Fermi pockets predicted by LDA calculations (in Fig. 1, M corresponds to the $[0; \pi]$, $[\pi; 0]$ points of the unfolded Brillouin zone), but generates only one hole pocket at Γ (i.e., near $[\pi; \pi]$). We expect the absence of a second hole pocket to play a minor role in the qualitative aspects of the pairing mechanism, as one pocket is enough for capturing the physics stemming from the approximate nesting between the electron and the hole Fermi pockets.

To place our effective model in the context of similar two-band models for the iron-based superconductors, we show in Fig. 2 a comparison with the $d_{zx} - d_{zy}$ model from Refs. 25,26,27. The high energy bands, $E_1(k)$ and $E_+(k)$, respectively, which are responsible for the formation of the electron pockets have the same energy scale and very similar dispersions. By contrast, the low-energy band $E_-(k)$ of the $d_{zx} - d_{zy}$ model has a characteristic energy that is an order of magnitude larger than the low-energy band $E_2(k)$ of the present model. Particularly significant is the rapid dispersion of $E_-(k)$ in the vicinity of $[\pi; \pi]$, which results, on the one hand, in a much larger Fermi energy for the hole pocket and, on the other hand, in smaller values of the susceptibility. Our model correctly takes into account the results of band structure calculations that give characteristic Fermi energies of about 0.2 eV for both types of pockets.

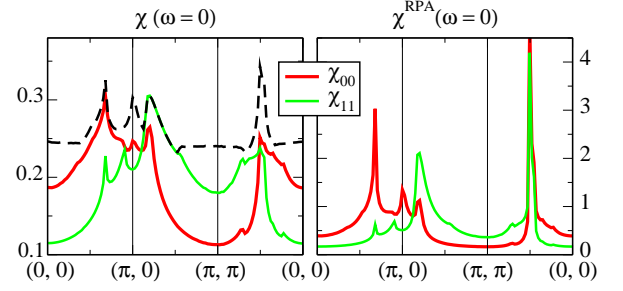


FIG. 3: (color online): Left panel: static spin susceptibility (χ_{00} —red line) and static transverse orbital susceptibility (χ_{11} —green line) for the two-orbital model studied in Ref. 26. The dash line represents the maximum eigenvalue of the matrix. Right panel: largest components of the spin-orbital susceptibility matrix in the RPA approximation. Notice that both $\chi_{00}^{(s)}$ and $\chi_{11}^{(s)}$ diverge near $(\pi, \pi) = (2, 2)$, signaling the presence of an instability. The instability is produced by the coupling of the spin ($s=0$) and transverse spin-orbital ($s=1$) modes, due to a non-vanishing χ_{01} .

IV. RPA SUSCEPTIBILITIES AND EFFECTIVE PAIRING INTERACTIONS

The random phase approximation (RPA) involves the summation of the whole series of bubble diagrams and, within the formalism described in Section II, it corresponds to the multiplication with the matrix $1 + \chi^{(c=s)}(q)^{-1}$. The result depends critically on the structure of the matrices $\chi^{(c=s)}$ and (q) . Let us consider the case corresponding to our model (and also to the degenerate orbital model), when the inter-orbital hybridization is real and has even parity, i.e., $t_{12}(k) = t_{12}(k)$. Within the SU(4) formalism, the coupling constant matrix is diagonal, with components given by Eq. (6), while the bare susceptibility matrix has the form

$$= \begin{pmatrix} 0 & 0 & 0 & 1 \\ \chi_{00} & \chi_{10} & \chi_{01} & \chi_{03} \\ 0 & 0 & \chi_{22} & 0 \\ \chi_{30} & \chi_{31} & 0 & \chi_{33} \end{pmatrix} \begin{pmatrix} 1 \\ C \\ A \\ B \end{pmatrix}; \quad (13)$$

where the nonvanishing components are

$$\begin{aligned} \chi_{00}(33) &= \frac{1}{2} (e_{11;11} + e_{22;22} - 2e_{2;21}); \\ \chi_{11}(22) &= e_{11;22} - e_{2;21}; \\ \chi_{03} &= \chi_{30} = \frac{1}{2} (e_{11;11} - e_{22;22}); \\ \chi_{01} &= \chi_{10} = e_{11;12} + e_{22;21}; \\ \chi_{31} &= \chi_{13} = e_{11;12} - e_{22;21}; \end{aligned} \quad (14)$$

Note that the transverse orbital component χ_{22} is decoupled from the other channels and its RPA value will depend only on $\chi_{22}^{(c=s)}$. By contrast, the spin (charge) susceptibility χ_{00} always couples to the longitudinal orbital

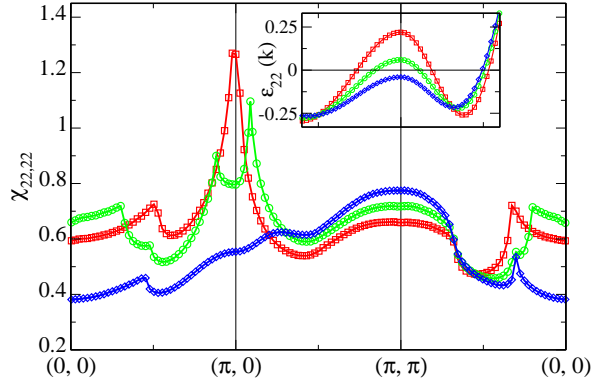


FIG. 4: (color online): Intra-orbital susceptibility $\chi_{22;22}$ corresponding to three different sets of hopping parameters $(t_{ij}^{22})_x$, $x = 2, f, g$, for the second orbital (see main text). The corresponding dispersion curves in the vicinity of $(\pi, 0)$ (i.e., $[\pi; 0]$) are shown in the inset and are characterized by () a large hole pocket (red squares), () small hole pocket (green circles), or () no hole pocket (blue diamonds). The existence of the hole pocket determines the appearance of peaks in the susceptibility near $[\pi; 0]$, due to an approximate nesting between the electron and the hole Fermi surfaces.

component χ_{33} . In addition, in the presence of an inter-orbital hybridization, these two components are coupled to the transverse orbital susceptibility χ_{11} . All these couplings can significantly enhance the susceptibilities. To give an example, we show in Fig. 3 the static spin susceptibility χ_{00} ($\neq 0$) and the transverse orbital susceptibility χ_{11} ($\neq 0$) for the two-band model studied in Ref. 26. The maximal eigenvalue of the susceptibility matrix (dashed line in Fig. 3) is peaked near $q = [\pi; \pi]$ as a result of the mixing between χ_{00} and χ_{11} . Note that $\chi_{01(10)}(q) \neq 0$ while $\chi_{31(13)}(q) = \chi_{30(03)}(q) = 0$ because of symmetry. At the RPA level, for an interaction $U = U^0 = 2.8$ and $J = J^0 = 0$ both χ_{00} and χ_{11} are strongly peaked near q (right panel in Fig. 3), indicating the proximity of a spin-orbital instability. This instability is the result of the spin channel ($\ell = 0$) being coupled to one of the transverse spin-orbital channels ($\ell = 1$) due to the hybridization between orbitals. The strength of this coupling is determined by the off-diagonal susceptibility $\chi_{01(10)}$. Note that the numerical value of $\chi_{01(10)}$ is negligible everywhere except in the vicinity of q where it has a peak $\chi_{01(10)} \approx 0.1$.

Next, we turn our attention to the RPA analysis of the effective two-band model described in the previous section. Using this simple model we want to address two basic questions: i) what is the dominant pairing channel, and ii) what is the specific contribution of the orbital degrees of freedom. We find that the physics of the two-band model is rather non-universal, depending strongly on both the structure of the non-interacting Hamiltonian and the form of the interaction. However, within a reasonable parameter window we find that (i) the dominant pairing channel is the orbital-triplet spin-singlet channel, and that (ii) the spin and orbital components are

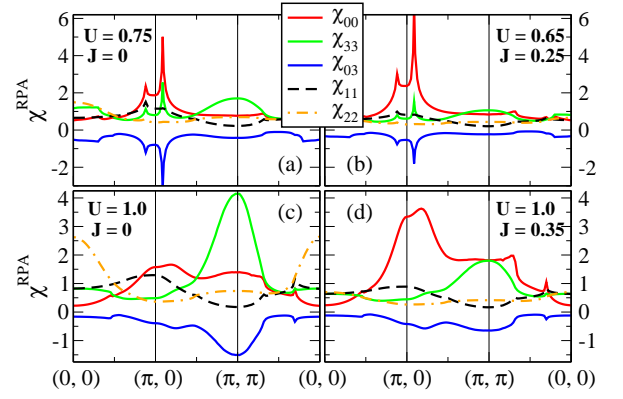


FIG. 5: (color online): RPA susceptibilities in the spin sector for various parameters of the two-orbital model: a) Band structure with a small hole FS and no Hund's coupling. b) Model with a small hole pocket and large Hund's coupling. c) No hole pocket and $J = 0$. d) No hole pocket and large Hund's coupling. Note that the mixing between the pure spin and the longitudinal orbital-spin components, measured by χ_{03} , is particularly strong in the absence of a strong Hund's coupling.

strongly coupled and typically give comparable contributions to the effective pairing interaction W . The relative weight of the spin channel is enhanced by increasing the size of the hole pocket, which leads to nesting, and by increasing the Hund's coupling J . In the opposite limit the orbital effects become dominant. In addition, we note that the symmetry of the hybridization, which determines the off-diagonal susceptibility χ_{1221} , plays a crucial role in determining the relative strength of various contributions. Our present choice, $\chi_{12}(k+Q) = \chi_{12}(k)$ for $Q = (\pi; 0)$ or $Q = (0; \pi)$, enhances the spin component over the orbital-spin contributions. By contrast, an even symmetry choice would further enhance the role of orbital fluctuations. We show that these coupled spin-orbital fluctuations are important and cannot be ignored in intrinsically multi-orbital systems like the iron-based superconducting oxides. In terms of the general scenarios described at the end of section II, we find scenario B as the most likely to be realized within our effective two-orbital model.

The first step in the RPA analysis involves the calculation of the bare susceptibilities $\epsilon_{ij;i'j'}^0$ for each of the three sets of parameters describing our two-orbital model, which were discussed in section III. The most significant parameter dependence is seen in $\epsilon_{22;22}$ as the second orbital is responsible for the existence and size of the hole pocket. We show in Fig. 4 the intra-orbital susceptibility $\epsilon_{22;22}$ corresponding to the three different sets of hopping parameters t_{ij}^{22} , $x = 2, f, g$. The case () corresponds to a large hole pocket (see the inset of Fig. 4) that produces an approximate nesting with the electron pocket and generates a strong peak at $[\pi; 0]$. This feature becomes weaker as the hole pocket shrinks – case () – and eventually disappears in the absence of

the hole pocket – case () – being replaced by a wide maximum near $[\pi; 0]$.

What happens in the presence of an interaction? To reduce the number of independent parameters we only consider the case

$$U^0 = U - 2J; \quad J^0 = J:$$

In the absence of Hund's coupling, $J = 0$, the RPA spin channel susceptibility $\chi^{(s)}(q)$ diverges at the critical values of the interaction $U_c^{(s)} = 0.75$, $U_c^{(s)} = 0.85$ and $U_c^{(s)} = 1.2$ for the three sets of orbital parameters, respectively. In the presence of a hole pocket the instability occurs in the vicinity of $[\pi; 0]$, while if only the electron pockets exist, the instability occurs at $[\pi; \pi]$. In both cases there is a strong mixing between the pure spin and the longitudinal orbital-spin components while the transverse orbital-spin components are practically decoupled. Including a Hund's coupling J strengthens the $[\pi; 0]$ instability or replaces the orbital-driven $[\pi; \pi]$ instability with a spin-driven $[\pi; 0]$ instability. The general trends of the RPA susceptibility are shown in Fig. 5 for band structures corresponding to two sets of band parameters, (small hole pocket) and (no hole pocket), and interactions characterized by either $J = 0$ or by a relatively strong Hund's coupling, $J=U = 0.35$. We note that a non-vanishing J always enhances the spin susceptibility, while suppressing the longitudinal orbital-spin component. However, in a more realistic model exchange interactions between nearest-neighbor and next-nearest-neighbor sites have to be considered^{17,18,19,21}. In this case, the bare coupling constant matrices $U^{(c=s)}$ will acquire momentum dependent contributions $J(q)$. Depending on the character (ferromagnetic, antiferromagnetic or mixed) of the exchange couplings, the spin susceptibility can be further enhanced or, by contrary, suppressed in favor of the orbital components. We stress that the inclusion of the exchange interaction is crucial, as it can qualitatively change the susceptibilities and, implicitly, the nature of the possible instabilities and that of the pairing mechanism.

We turn now our attention to the calculation of the effective pairing interaction W_{ab} given by Eqns. (9) and (10). We show in Fig. 6 the momentum dependence of the dominant effective couplings. The largest component is always the second diagonalelement of the orbital-triplet spin-singlet matrix, $[W_{ts}]_{22}$. In the absence of a hole pocket, for $J = 0$ (panel (c) in Fig. 6), $[W_{ts}]_{22}(k)$ has a wide maximum at $(\pi; \pi)$, while the other effective couplings have a much weaker momentum dependence. By contrast, if the hole pocket exists (panels (a) and (b)), $[W_{ts}]_{22}(k)$ is characterized by sharp maxima in the vicinity of $(\pi; 0)$. These maxima are the consequence of the approximate nesting between the hole and electron Fermi surfaces. Note that the orbital-triplet spin-singlet pair operator (7) is an even function of momentum. Consequently, because of the of the structure near $(\pi; 0)$, the superconducting gap will have s-type symmetry with opposite signs on the hole and electron pockets.

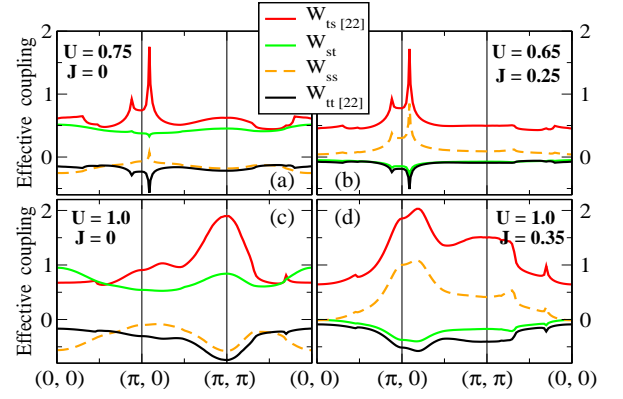


FIG. 6: (color online): Momentum dependence of the dominant components of the effective coupling for the parameter regimes of Fig. 5. Note that the largest effective interaction occurs in the orbital-triplet spin-singlet channel (red line) and, in the presence of a hole pocket – (a) and (b) – it leads to s-wave pairing with opposite signs of the gap on the electron and hole Fermi surfaces. The orbital dominated case (c) is consistent with d-wave pairing, while in case (d) there are several competing channels.

By contrast, in the absence of the hole pockets and for $J = 0$, the $(\pi; \pi)$ maximum will enforce a d-type symmetry. The experimental evidence for the gap symmetry is rather contradictory. Some point-contact Andreev reflection experiments^{31,32}, as well as microwave³³ and ARPES^{34,35} measurements suggest fully-gaped superconductivity, which is consistent with s-wave pairing. On the other hand, the results of other point-contact Andreev reflection experiments³⁶, together with NMR results³⁷ and Hc1 magnetization measurements³⁸ suggest a nodal gap function, consistent with d- or p-wave pairing. Clearly, further work is necessary in order to clarify this problem. Note that, regardless of symmetry, if pairing occurs in the orbital-triplet spin-singlet channel it originates in the $d_{zx} - d_{yz}$ "effective" orbital. However, because the off-diagonalelements $[W_{ts}]_{12} = [W_{ts}]_{21}$ are non-zero, pairing is also induced in the d_{xy} orbital. Therefore, the resulting pairing gap has two components which are characterized by two different energy scales that can be obtained by numerically solving a matrix gap equation. The gap equation can be derived using standard procedures from a BCS-type mean field approximation of the effective Hamiltonian (8). Notice that for large Hund's couplings (panels (b) and (d) in Fig. 6) the relation $J > U^0$ is satisfied and the coupling constant in the orbital-singlet spin-triplet channel W_{st} becomes negative²², opening the possibility of s-wave pairing in this channel. Nonetheless, in the presence of a hole pocket – case (b) – because of the dominant contribution from $[W_{ts}]_{22}$, pairing realizes in the orbital-triplet spin-singlet channel. On the other hand, in case (d) – with no hole pocket and strong J – there are several closely competing channels. Finally, we note that for most of the parameter space our model predicts intra-orbital, rather than inter-orbital pairing. If

the Hund's coupling is small, scenario B is realized and pairing occurs in the orbital-triplet spin-singlet channel with t_{2g} as the strongest component. For large J , in the presence of a hole pocket, the relative importance of the off-diagonal susceptibility $\chi_{12,21}$ diminishes and scenario A is realized. However, pairing still occurs in the orbital-triplet spin-singlet channel and is dominated by the second intra-orbital component. The only possibility for inter-orbital pairing occurs in the absence of a hole pocket and for large Hund's couplings, when pairing may occur in the orbital-singlet spin-singlet or in the orbital-singlet spin-triplet channels, depending on the details of the model. However, we emphasize again that these results are highly non-universal and they strongly depend, for example, on the number of orbitals considered, on the symmetry and strength of the hybridization, or on the values of possible non-local interactions.

V. SUMMARY AND CONCLUSIONS

In summary, we propose a paradigm for superconductivity in the new Fe-based materials where the pairing is caused by orbital fluctuations strongly coupled to spin fluctuations in the renormalized multiband ground state. We test our theoretical idea by carrying out an RPA-type calculation using a minimal two-orbital model consistent with the low energy bands determined by first principles band structure calculations. We find that the intra-

orbital pairing, rather than the inter-orbital or the inter-band pairings, mediated by coupled spin-orbital fluctuations is the driving mechanism here. One specific falsifiable prediction of our paradigm is that, if the parent compound is not multiband (thus, rendering orbital fluctuations relatively unimportant), then the system would not be superconducting (or will have a rather low transition temperature). Our numerical analysis of the effective two-orbital model suggests several tasks and directions for future studies: i) It is crucial to determine the size of the Fermi surfaces and the relative strength of the quasiparticles on the electron and hole pockets for a relevant doping range. If, for example, the quasiparticle residue takes significantly different values on the two types of Fermi surfaces, all the features coming from their approximate nesting will be strongly suppressed. ii) It is necessary to know exactly the symmetry of the inter-orbital hybridization and to have a good estimate of its strength. A model that just reproduces the correct low-energy band structure is not necessarily correct. The symmetry of the inter-orbital mixing terms plays a key role in establishing the relative weight and the couplings between various spin, charge and orbital modes. iii) A realistic tight-binding model of the Fe-pnictides should include short-range interaction terms. The nature and the strength of these interactions have direct consequences on the possible instabilities, as well as on the superconducting mechanism.

This work was supported by LPS-NSA-CMTC.

-
- ¹ Y. Kamihara, T. Watanabe, M. Hirano, and H. Hosono, *J. Am. Chem. Soc.* **130**, 3296 (2008).
 - ² G. Mu, X. Zhu, L. Fang, L. Shan, C. Ren, and H.-H. Wen, *Chin. Phys. Lett.* **25**, 2221 (2008).
 - ³ H.-H. Wen, G. Mu, L. Fang, H. Yang, and X. Zhu, *Europhys. Lett.* **82**, 17009 (2008).
 - ⁴ X. H. Chen, T. Wu, G. Wu, R. H. Liu, H. Chen, and D. F. Fang, *Nature* **453**, 761 (2008).
 - ⁵ G. F. Chen, Z. Li, D. Wu, G. Li, W. Z. Hu, J. Dong, P. Zheng, J. L. Luo, and N. L. Wang, *Phys. Rev. Lett.* **100**, 247002 (2008).
 - ⁶ Z.-A. Ren, J. Yang, W. Lu, W. Yi, G.-C. Che, X.-L. Dong, L.-L. Sun, and Z.-X. Zhao, *arXiv:0803.4283* (2008).
 - ⁷ Z.-A. Ren, G.-C. Che, X.-L. Dong, J. Yang, W. Lu, W. Yi, X.-L. Shen, Z.-C. Li, L.-L. Sun, F. Zhou, et al, *Materials Research Innovations* **12**, 105 (2008).
 - ⁸ C. Wang, L. Li, S. Chi, Z. Zhu, Z. Ren, Y. Li, Y. Wang, X. Lin, Y. Luo, X. Xu, et al, *Europhys. Lett.* **83**, 67006 (2008).
 - ⁹ D. Singh and M. Du, *Phys. Rev. Lett.* **100**, 237003 (2008).
 - ¹⁰ L. Boeri, O. V. Dolgov, and A. A. Golubov, *Phys. Rev. Lett.* **101**, 026403 (2008).
 - ¹¹ I. Mazin, D. Singh, M. Johannes, and M. Du, *Phys. Rev. Lett.* **101**, 057003 (2008).
 - ¹² C. Cao, P. J. Hirschfeld, and H.-P. Cheng, *Phys. Rev. B* **77**, 220506(R) (2008).
 - ¹³ K. Kuroki, S. Onari, R. Arita, H. Utsui, Y. Tanaka, H. Kon-tani, and H. Aoki, *Phys. Rev. Lett.* **101**, 087004 (2008).
 - ¹⁴ T. Nomura, S. W. Kim, Y. Kamihara, M. Hirano, P. V. Sushko, K. Kato, M. Takata, A. L. Shluger, and H. Hosono, *arXiv:0804.3569* (2008).
 - ¹⁵ K. Haule, J. H. Shim, and G. Kotliar, *Phys. Rev. Lett.* **100**, 226402 (2008).
 - ¹⁶ C. de la Cruz, Q. Huang, J. W. Lynn, J. Li, W. R. II, J. L. Zarestky, H. A. Mook, G. F. Chen, J. L. Luo, N. L. Wang, et al, *Nature* **453**, 899 (2008).
 - ¹⁷ Q. Si and E. Abraham, *Phys. Rev. Lett.* **101**, 076401 (2008).
 - ¹⁸ T. Yildirim, *Phys. Rev. Lett.* **101**, 057010 (2008).
 - ¹⁹ V. Cvetkovic and Z. Tesanovic, *arXiv:0804.4678v3*.
 - ²⁰ Y. Yamashita and K. Ueda, *Phys. Rev. B* **67**, 195107 (2003).
 - ²¹ K. Haule and G. Kotliar, *arXiv:0805.0722* (2008).
 - ²² P. A. Lee and X.-G. Wen, *arXiv:0804.1739v2* (2008).
 - ²³ X. Dai, Z. Fang, Y. Zhou, and F.-C. Zhang, *Phys. Rev. Lett.* **101**, 057008 (2008).
 - ²⁴ Z.-H. Wang, H. Tang, Z. Fang, and X. Dai, *arXiv:0805.0736* (2008).
 - ²⁵ S. Raghu, X.-L. Qi, C.-X. Liu, D. Scalapino, and S.-C. Zhang, *Phys. Rev. B* **77**, 220503 (2008).
 - ²⁶ X.-L. Qi, S. Raghu, C.-X. Liu, D. J. Scalapino, and S.-C. Zhang, *arXiv:0804.4332v2* (2008).
 - ²⁷ M. Daghofer, A. Moreo, J. A. Riera, E. Arrigoni, D. Scalapino, and E. Dagotto, *arXiv:0805.0148v2* (2008).
 - ²⁸ Y. Wan and Q.-H. Wang, *arXiv:0805.0923v3* (2008).
 - ²⁹ T. Li, *arXiv:0804.0536v1* (2008).

- ³⁰ K. Nakamura, R. Arita, and M. Imada, J. Phys. Soc. Jpn. 77, 093711 (2008).
- ³¹ T. Y. Chen, Z. Tesanovic, R. H. Liu, X. H. Chen, and C. L. Chien, Nature 453, 1224 (2008).
- ³² P. Samuely, P. Szabo, Z. Pribulova, M. E. Tillman, and S. B. P. C. Canfield, arXiv:0806.1672v3 (2008).
- ³³ K. Hashimoto, T. Shibauchi, T. Kato, K. Ikada, R. Okazaki, H. Shishido, M. Ishikado, H. Kito, A. Iyo, H. Eisaki, et al., arXiv:0806.3149v3 (2008).
- ³⁴ H. Ding, P. Richard, K. Nakayama, T. Sugawara, T. Arakane, Y. Sekiba, A. Takayama, S. Souma, T. Sato, T. Takahashi, et al., Europhysics Letters 83, 47001 (2008).
- ³⁵ L. Wray, D. Qian, D. Hsieh, Y. Xia, L. Li, J. Checkelsky, A. Pasupathy, K. Gomes, A. Fedorov, G. Chen, et al., arXiv:0808.2185v1.
- ³⁶ L. Shan, Y. Wang, X. Zhu, G. Mu, L. Fang, C. Ren, and H. H. Wen, Europhys. Lett. 83, 57004 (2008).
- ³⁷ K. Matano, Z. Ren, X. Dong, L. Sun, Z. Zhao, and G. Qing Zheng, Europhys. Lett. 83, 57001 (2008).
- ³⁸ Z. A. Ren, W. Lu, J. Yang, W. Yi, X.-L. Shen, Z.-C. Li, G.-C. Che, X.-L. Dong, L.-L. Sun, F. Zhou, et al., Chin. Phys. Lett. 25, 2215 (2008).